

Towards Attribution of Generators and Emotional Manipulation in Cross-Lingual Synthetic Speech using Geometric Learning

Girish^{1*}, Mohd Mujtaba Akhtar^{2*}, Farhan Sheth³, Muskaan Singh⁴

¹UPES, India, ²V.B.S.P.U, India, ³Manipal University Jaipur, India, ⁴Ulster University, UK,

Correspondence: m.singh@ulster.uk.in

Abstract

In this work, we address the problem of fine-grained traceback of emotional and manipulation characteristics from synthetically manipulated speech. We hypothesize that combining semantic–prosodic cues captured by Speech Foundation Models (SFM) with fine-grained spectral dynamics from auditory representations can enable more precise tracing of both emotion and manipulation source. To validate this hypothesis, we introduce MiCuNet, a novel multitask framework for fine-grained tracing of emotional and manipulation attributes in synthetically generated speech. Our approach integrates SFM embeddings with spectrogram-based auditory features through a mixed-curvature projection mechanism that spans Hyperbolic, Euclidean, and Spherical spaces guided by a learnable temporal gating mechanism. Our proposed method adopts a multitask learning setup to simultaneously predict original emotions, manipulated emotions, and manipulation sources on the Emo-Fake dataset (EFD) across both English and Chinese subsets. MiCuNet yields consistent improvements, consistently surpassing conventional fusion strategies. To the best of our knowledge, this work presents the first study to explore a curvature-adaptive framework specifically tailored for multitask tracking in synthetic speech.

1 Introduction and Related Work

The rapid evolution of synthetic speech technologies has ushered in a new era of expressive and adaptable voice generation systems. Among these, emotional voice conversion (EVC) has emerged as a particularly transformative advancement, enabling the alteration of emotional tone in speech while preserving the speaker’s identity and linguistic integrity. Recent advances in synthetic speech generation have raised new challenges not only

for detecting manipulated audio but also for tracing the original characteristics embedded within it. Early research efforts, notably the ASVspoof series (Wu et al., 2015; Kinnunen et al., 2017; Todisco et al., 2019; Yamagishi et al., 2021), laid a strong foundation for detecting spoofed speech, initially targeting synthetic speech generated via text-to-speech (TTS) and voice conversion (VC) systems, and gradually expanding to address more realistic replay attacks and deepfake scenarios. (Yamagishi et al., 2021) introduced additional challenges involving deepfake audio, compression artifacts, and mismatched telephony conditions, underscoring the growing sophistication of modern spoofing attacks. In parallel, Müller et al. (2024) systematically evaluated the generalization limits of audio deepfake detectors, exposing critical vulnerabilities when models trained on controlled datasets were tested on in-the-wild samples. Beyond authenticity verification, research has increasingly shifted towards fine-grained emotion modeling. Recent works such as pre-finetuning approaches for emotional speech recognition (Chen and Yu, 2023) and emotion prompting techniques (Zhou et al., 2023) demonstrate the benefits of task adaptation and multi-task learning to capture subtle emotional cues. Emotional manipulation in synthetic speech has also gained attention, with advances in controllable emotional voice conversion (Qi et al., 2024) and fine-grained emotion control in voice cloning systems like EmoKnob (Chen et al., 2024).

(Han et al., 2025) showed that self-supervised models match human performance in cross-lingual SER, albeit with notable dialectal variability. Complementing this, (Upadhyay et al., 2024) proposed a layer anchoring approach to enhance generalization by aligning internal transformer layers across languages. (Baklouti et al., 2024) further addressed the domain mismatch using MMD-based transfer learning with 2D spectrograms, specifically targeting low-resource emotion transfer. Multitask learn-

*Equal Contribution as first authors

ing (MTL) has emerged as an effective strategy to improve SER by encouraging the model to learn shared structures across related tasks. A recent MTLSER framework (Chen et al., 2025) co-learned emotional and auxiliary cues to improve prediction robustness, while (Wang and Shen, 2024) integrated speech feature enhancement into a soft decision tree–LSTM hybrid. Coordinate attention mechanisms have also been explored in multitask setups, such as in the work of (Sun et al., 2025), where SER accuracy was improved by adaptively focusing on salient emotional regions. The structural properties of emotion space have prompted research into non-Euclidean embeddings. (Araño et al., 2021) explore hyperbolic geometry for multimodal sentiment and emotion classification, revealing that hierarchical relationships between emotional states can be better preserved in hyperbolic space. This line of work provides a strong precedent for our own investigation into mixed-curvature manifold representations. Recent advances in emotional speech synthesis underscore the growing concern over emotionally manipulated audio. (Zhu et al., 2024) presents METTS, a multilingual text-to-speech model capable of disentangling speaker identity, language, and emotion to support high-fidelity emotional speech synthesis across speakers and languages. Extending this, (Li et al., 2023) introduces a zero-shot framework for cross-lingual emotion transfer, using predictive coding and hierarchical emotion modeling to synthesize expressive speech in unseen languages without emotional supervision. However, existing approaches largely focus either on binary detection or broad categorization, leaving the fine-grained traceback of original emotional states in manipulated speech largely unexplored. Addressing this critical gap, we propose **MiCuNet** (**Mixed-Curvature Network**) for a synthetic speech framework designed for fine-grained emotion and tracing of manipulation source from synthetic speech.

Beyond authenticity verification, research has increasingly shifted towards fine-grained emotion modeling. *We hypothesize that leveraging SFMs together with rich spectrogram-based auditory features has an ability. As synthetic speech systems become increasingly indistinguishable from natural speech, the need for granular interpretability and attribution in detection frameworks becomes not only relevant but imperative. For the recognition of the original emotional state, the manipulated current emotion, and the underlying manipulation*

source model. To validate this hypothesis, we propose **MiCuNet**, a mixed-curvature feature fusion framework that systematically integrates these diverse representations under a multitask learning objective. To evaluate our hypothesis, we carry out a comprehensive comparison of state-of-the-art speech foundation models, including multilingual, monolingual, and speaker recognition pretraining paradigms. We integrate embeddings extracted from x-vector, MMS, XLS-R, Whisper, WavLM, and Wav2Vec 2.0 with spectrogram-based auditory representations obtained through STFT, CQT, and Wavelet transforms. This diverse feature integration is projected through the **MiCuNet** framework under a mixed-curvature multitask learning setup to enable fine-grained tracing of emotional and manipulation characteristics from synthetic speech.

To summarize, key contributions of this work are as follows: (i) To the best of our knowledge, we are the first large-scale and systematic study exploring the effectiveness of SFMs for fine-grained emotion and manipulation source tracing from synthetically manipulated speech. Our experiments reveal that multilingual SFMs consistently outperform monolingual and speaker recognition models across both English and Chinese subsets. To this end, our work represents the first exploration of Speech foundation models for the traceback for the source-attributes task on the EmoFake dataset, a direction previously unexplored. (ii) We propose a novel fusion framework, **MiCuNet**, which synchronizes embeddings through a mixed-curvature projection into three geometric spaces such as Hyperbolic, Euclidean, and Spherical via a learnable gating mechanism. Through **MiCuNet**, we achieve superior performance compared to individual SFMs and standard fusion baselines, setting a new benchmark for fine-grained emotional forgery detection (EFD) in synthetic speech.

All resources (code, configs, and model weights) are available at:¹

2 Representations

In this section, we describe the detailed representations of the speech foundation models (SFMs) and spectrogram features adopted in our approach.

Speech PTMs: We use wav2vec 2.0² (Baevski

¹<https://github.com/Helexometry/MiCuNet-IJCNLP-AACL>

²<https://huggingface.co/facebook/wav2vec2-base>

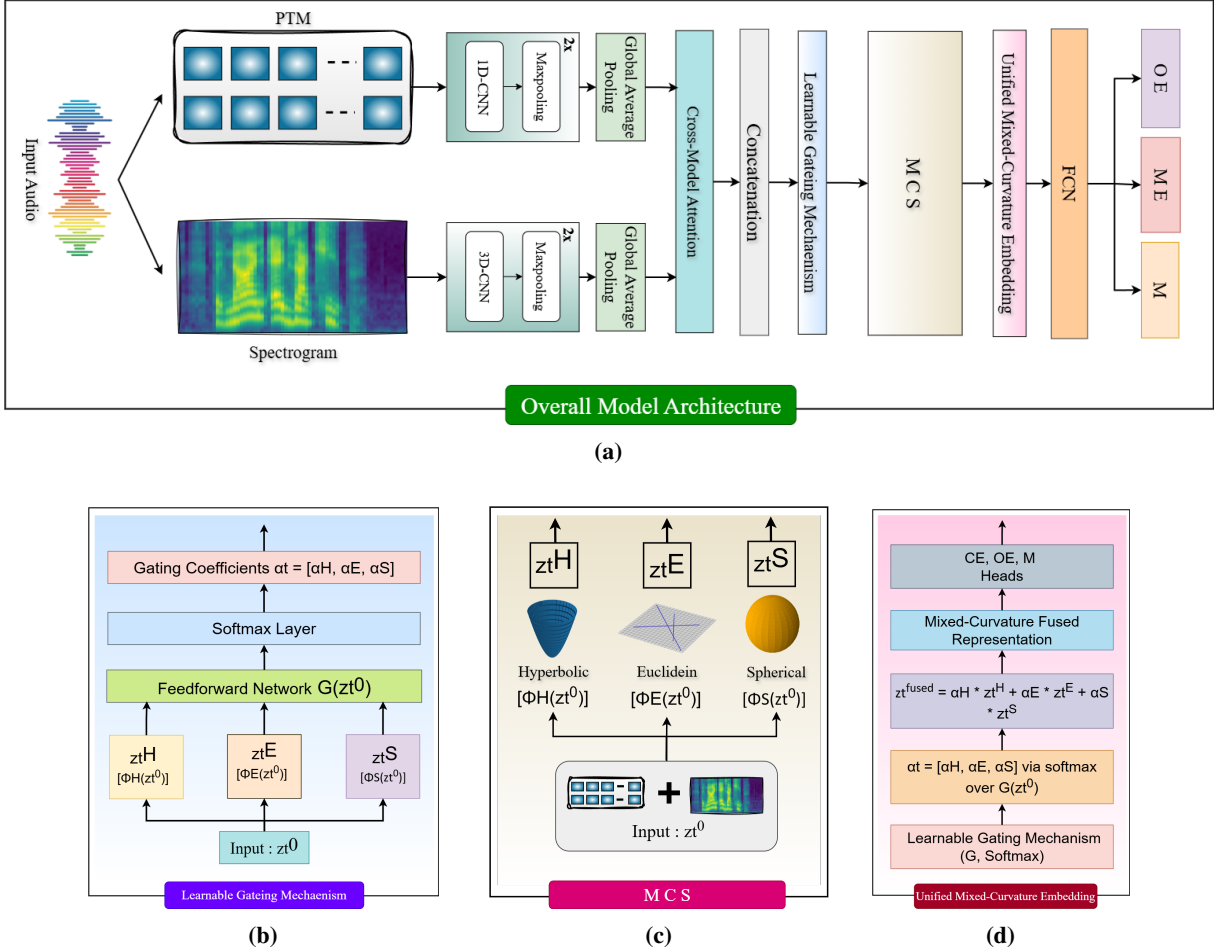


Figure 1: The MiCuNet architecture. (a) Full pipeline: modality-specific encoders process PTM and spectrogram features using 1d and 3d CNNs, respectively, followed by self-attention, cross-modal attention, concatenation, and a curvature-aware fusion module. (b) Learnable Gating Mechanism: generates dynamic weighting coefficients for each manifold space using a feedforward network and a softmax layer. (c) Mixed-Curvature Projection: input representation is projected in parallel onto hyperbolic, Euclidean, and spherical manifolds using shared transformation layers. (d) Unified Fusion Head: weighted combination of manifold-specific embeddings followed by multitask heads for OE, CE, and M prediction.

et al., 2020), wavLM³ (Chen et al., 2022), MMS⁴ (Pratap et al., 2024), we use XLS-R⁵ (Babu et al., 2022), x-vector⁶ (Snyder et al., 2018), and Whisper⁷ (Radford et al., 2023) as our speech foundation models. wav2vec 2.0 and wavLM are self-supervised PTMs trained on 53k and 94k hours of unlabeled audio, respectively, solving masked prediction tasks. wavLM further includes speech denoising during pretraining and improves generalization across tasks. MMS is trained on 1400 languages with 49k hours of labeled and 55k hours of unlabeled data and built on wav2vec 2.0 backbone. XLS-R extends wav2vec 2.0 to 128 languages us-

ing a multilingual contrastive learning setup. Whisper is trained in a fully supervised manner on 680k hours of web data for ASR, VAD, translation, and language ID. X-vector is a TDNN model trained on VoxCeleb1+2 for speaker verification. We use base versions of wav2vec 2.0 and wavLM (trained on English LibriSpeech). For feature extraction, we average pool the last hidden layer of all models. For Whisper, we extract from the encoder output. Audio is resampled to 16kHz. Representation dimensions are: 768 (wav2vec 2.0, wavLM), 1280 (MMS, XLS-R), 512 (x-vector, Whisper).

Spectrogram Features: We use handcrafted features extracted from three time-frequency transforms—STFT (Allen and Rabiner, 1977), CQT (Brown, 1991), and WT (Mallat, 1989)—combined with four auditory filterbanks: Mel, Gammatone, Linear, and DCT.

³<https://huggingface.co/microsoft/wavlm-base>

⁴<https://huggingface.co/facebook/mms-1b>

⁵huggingface.co/...xls-r-300m

⁶<https://huggingface.co/speechbrain/spkrec-xvect-voxceleb>

⁷<https://huggingface.co/openai/whisper-base>

PTMs	E												C														
	OE			CE			M			OE			CE			M			OE			CE			M		
	A	F1	EER																								
W2	69.67	68.36	11.18	78.82	77.62	7.09	76.94	75.25	9.76	67.81	66.37	11.69	77.28	76.64	7.44	75.68	74.29	11.69	75.68	74.29	11.69	72.73	71.68	13.45			
WL	64.05	62.91	12.88	75.28	74.61	9.68	74.52	74.68	10.09	63.84	62.51	13.45	74.67	73.29	10.17	72.73	71.68	13.45	72.73	71.68	13.45	71.68	70.53	11.69			
MM	81.90	80.44	5.29	87.45	86.98	3.41	85.22	83.10	3.95	78.89	77.09	5.63	84.01	82.09	3.58	81.19	79.65	5.63	81.19	79.65	5.63	79.65	78.03	3.58			
XL	79.54	77.12	6.40	85.32	84.23	4.09	81.70	79.16	4.49	72.49	71.12	6.76	82.93	80.99	4.29	77.69	76.14	6.76	77.69	76.14	6.76	76.14	74.84	6.76			
W	60.93	59.50	13.56	65.78	64.40	10.73	63.20	62.75	7.29	59.68	58.24	14.19	64.81	63.36	11.28	62.45	61.89	14.19	62.45	61.89	14.19	61.89	60.93	14.19			
XV	58.65	57.24	14.51	63.58	62.32	11.33	61.88	60.79	8.26	56.68	55.69	15.14	62.57	61.64	11.82	60.99	59.47	15.14	60.99	59.47	15.14	59.47	58.65	15.14			
S-LI	78.56	77.54	7.41	81.23	80.12	3.53	79.82	78.45	5.47	77.26	77.72	7.78	80.03	79.85	3.71	78.72	78.20	7.78	78.72	78.20	7.78	78.20	77.56	3.71			
S-ME	75.23	73.11	8.05	76.34	74.32	5.18	77.41	75.23	6.29	74.13	73.28	8.44	74.94	74.10	5.40	76.21	75.05	8.44	76.21	75.05	8.44	75.05	74.84	8.44			
S-GT	73.45	71.35	8.45	75.89	73.89	5.98	76.14	75.12	6.84	72.25	71.80	8.84	74.89	73.55	6.24	74.84	73.50	8.84	74.84	73.50	8.84	73.50	73.25	8.84			
C-ME	74.34	72.34	9.74	76.45	74.85	6.08	79.23	78.56	4.98	72.84	72.60	10.24	75.35	74.70	6.38	78.03	78.30	10.24	78.03	78.30	10.24	78.30	77.88	10.24			
C-GT	72.89	70.56	8.77	77.56	75.47	5.02	76.78	75.34	6.31	71.69	70.10	9.27	76.26	75.20	5.24	75.38	75.60	9.27	75.38	75.60	9.27	75.60	75.38	9.27			
C-LI	75.89	74.05	7.43	78.23	76.12	6.48	76.56	74.98	7.00	74.59	74.30	7.77	76.83	76.35	6.79	75.46	74.70	7.77	75.46	74.70	7.77	74.70	74.44	7.77			
W-ME	70.47	68.25	10.95	74.12	72.45	7.93	71.34	69.84	8.92	69.37	68.50	11.46	72.62	72.20	8.29	70.14	69.60	11.46	70.14	69.60	11.46	69.60	69.03	11.46			
W-GT	76.34	74.89	5.85	79.12	78.23	5.28	77.56	75.98	5.66	75.14	75.10	6.15	78.12	78.00	5.55	76.06	75.75	6.15	76.06	75.75	6.15	75.75	75.44	6.15			
W-LI	74.23	72.12	10.75	78.45	76.50	6.07	76.85	74.67	7.51	72.93	72.30	11.43	77.35	76.30	6.33	75.45	74.40	11.43	75.45	74.40	11.43	74.40	73.95	11.43			

Table 1: Multitask performance on English (E) and Chinese (C) corpora for the following pre-trained models (PTMs); Abbreviations used: Wav2vec 2.0 (W2), WavLM (WL), MMS (MS), XLS-R (XL), Whisper (W), XVector (XV); and using spectral/time-frequency features: Constant-Q Transform–Gammatone (CQT_GAMMATONE / C-GT), Constant-Q Transform–Linear (CQT_LINEAR / C-LI), Constant-Q Transform–Mel (CQT_ME / C-ME), Short-Time Fourier Transform–Gammatone (STFT_GAMMATONE / S-GT), Short-Time Fourier Transform–Linear (STFT_LINEAR / S-LI), Short-Time Fourier Transform–Mel (STFT_ME / S-MEL), Wavelet Transform–Gammatone (WT_GAMMATONE / W-GT), Wavelet Transform–Linear (WT_LINEAR / W-LI), Wavelet Transform–Mel (WT_ME / W-ME). Abbreviations: OE = Original–Emotion; CE = Current–Emotion; M = Model prediction; ACC = Accuracy; F1 = F1-score; EER = Equal Error Rate. Abbreviations used are consistent across Tables: 1,2,3,4,5,6.

3 Modeling

3.1 Individual Representation Modeling

For downstream classification, we use task-specific CNN architectures. The CNN consists of two 1d convolutional layers (64 and 128 filters, kernel size 3), each followed by ReLU activation and max pooling (pool size 2). The output is flattened and passed through a dense layer with 120 units (ReLU), followed by a softmax layer for classification. In parallel, for spectrogram-based auditory features, we implement a 3D CNN. The architecture comprises three convolutional blocks with increasing channel sizes ($32 \rightarrow 64 \rightarrow 128$). Each block includes a $3 \times 3 \times 3$ convolution, followed by batch normalization and a ReLU activation, and is then followed by a $2 \times 2 \times 2$ max pooling layer to reduce the spatial and temporal dimensions.

3.1.1 MiCuNet

To better preserve nuanced emotional and manipulation cues from synthetic speech, we introduced **MiCuNet**, a mixed-curvature projection and fusion network designed to preserve fine-grained emotional and manipulation cues in synthetic speech. The complete system is illustrated in Figure 1, where Figure 1a depicts the full end-to-end architecture and Figures 1b–1d shows the key internal modules.

Feature Extraction and Cross-Modal Alignment:

As illustrated in Figure 1a, we encode speech PTM

embeddings using a 1D-CNN and handcrafted spectrogram features using a 3D-CNN. To obtain fixed-dimensional representations, we apply global average pooling across each modality’s temporal and spatial dimensions. A cross-modal attention module enables bidirectional contextual interaction between modalities. The resulting vectors are concatenated to form the joint embedding \mathbf{z}^0 .

Mixed-Curvature Projection: As shown in Figure 1c, visualizes how \mathbf{z}^0 is projected in parallel onto hyperbolic, Euclidean, and spherical manifolds using shared nonlinear transformations:

$$\mathbf{z}^{\mathbb{H}} = \Phi^{\mathbb{H}}(\mathbf{z}^0), \quad \mathbf{z}^{\mathbb{E}} = \Phi^{\mathbb{E}}(\mathbf{z}^0), \quad \mathbf{z}^{\mathbb{S}} = \Phi^{\mathbb{S}}(\mathbf{z}^0) \quad (1)$$

Here, $\Phi^{\mathbb{H}}, \Phi^{\mathbb{E}}, \Phi^{\mathbb{S}}$ are nonlinear transformation functions projecting into hyperbolic, Euclidean, and spherical spaces, respectively.

To capture the diverse structural properties inherent in emotional and manipulation signals, we leverage these three fundamental geometric manifolds:

Hyperbolic Space (\mathbb{H}^n): We use the Poincaré ball model of hyperbolic space with Möbius geometry to capture hierarchical and tree-like relationships prevalent in manipulated speech structures. Let $\mathbb{D}^n = \{\mathbf{x} \in \mathbb{R}^n : \|\mathbf{x}\| < 1\}$ denote the unit ball. We employ Möbius addition \oplus , exponential map $\exp^{\mathbb{H}}$, and logarithmic map $\log_0^{\mathbb{H}}$ centered at the origin. The exponential map for projecting a Euclidean tangent vector \mathbf{v} onto the manifold is:

$$\exp_0^{\mathbb{H}}(\mathbf{v}) = \tanh(\sqrt{c}\|\mathbf{v}\|) \cdot \frac{\mathbf{v}}{\sqrt{c}\|\mathbf{v}\|} \quad (2)$$

The corresponding logarithmic map is:

$$\log_0^{\mathbb{H}}(\mathbf{x}) = \tanh^{-1}(\sqrt{c}\|\mathbf{x}\|) \cdot \frac{\mathbf{x}}{\sqrt{c}\|\mathbf{x}\|} \quad (3)$$

Here, c is the curvature (learned during training), and $\|\cdot\|$ denotes the Euclidean norm. The geodesic distance used in this space is:

$$d_{\mathbb{H}}(\mathbf{x}, \mathbf{y}) = \frac{2}{\sqrt{c}} \tanh^{-1}(\|\ominus \mathbf{x} \oplus \mathbf{y}\|) \quad (4)$$

This hyperbolic geometry enables MiCuNet to model manipulation intensities and depth transitions more effectively than Euclidean space alone.

Euclidean Space (\mathbb{E}^n): The Euclidean component of our mixed-curvature space serves as a conventional baseline for capturing linear interactions in the fused representation. No transformation is applied, and distances are measured using the L_2 norm:

$$d_{\mathbb{E}}(\mathbf{x}, \mathbf{y}) = \|\mathbf{x} - \mathbf{y}\|_2 \quad (5)$$

Euclidean embeddings complement the curvature-rich counterparts by retaining locality-sensitive structure in the feature space.

Spherical Space (\mathbb{S}^n): To capture cyclic or rotational patterns in emotional expression, we project part of the fused embedding onto a unit hypersphere of positive curvature. We use exponential and logarithmic maps centered at the north pole. The exponential map is defined as:

$$\exp_0^{\mathbb{S}}(\mathbf{v}) = \cos(\|\mathbf{v}\|) \cdot \mathbf{n} + \sin(\|\mathbf{v}\|) \cdot \frac{\mathbf{v}}{\|\mathbf{v}\|} \quad (6)$$

Here, \mathbf{n} denotes the north pole, and $\|\mathbf{v}\|$ is the norm of the tangent vector. The geodesic (angular) distance on the unit sphere is:

$$d_{\mathbb{S}}(\mathbf{x}, \mathbf{y}) = \arccos(\langle \mathbf{x}, \mathbf{y} \rangle) \quad (7)$$

This space supports modeling speaker-intrinsic cycles and oscillatory emotional trajectories that flat or hyperbolic spaces do not capture well.

By combining these spaces, the **MiCuNet** layer gains the capacity to model a broad spectrum of

geometric dependencies within the fused representation. Instead of relying on a single manifold, MiCuNet projects the joint embedding onto three complementary geometric spaces—*hyperbolic*, *spherical*, and *Euclidean*—each designed to capture different structural patterns in emotional speech. To fuse these manifold-specific embeddings into a unified representation, we map them into a common Euclidean space where standard arithmetic operations such as weighted summation can be applied. This transformation is achieved through logarithmic maps, which convert each curved-space embedding into its corresponding tangent space, effectively flattening the geometry for fusion. For a point x in the *hyperbolic space* \mathbb{H}^n , modeled via the *Poincaré ball* with curvature $c > 0$, the logarithmic map to the Euclidean tangent space at the origin is shown in equation 3.

Similarly, for a point x on the *unit hypersphere* \mathbb{S}^{n-1} , the mapping to the tangent space at the *north pole* n is:

$$\log_{\mathbb{S}}(x) = \theta \cdot \frac{x - \cos(\theta) \cdot n}{\sin(\theta)}, \quad (8)$$

where $\theta = \arccos(\langle x, n \rangle)$

Once all embeddings are aligned in this shared Euclidean space, **MiCuNet** performs a geometry-aware fusion using a learnable gating mechanism. This module dynamically assigns weights to each manifold’s contribution, allowing the model to emphasize the most informative geometry based on the task and input context. This fusion strategy not only enables richer representation learning but also enhances the model’s adaptability across different emotional, linguistic, and generative conditions.

Multitask Output Heads: As shown in Figure 1d, $\mathbf{z}_{\text{fused}}$ is passed to three independent fully-connected heads for joint prediction of Current Emotion (CE), Original Emotion (OE), and Manipulation source (M). Each head includes a hidden layer with ReLU activation followed by a softmax classifier. We specifically consider Euclidean, Hyperbolic, and Spherical spaces as they represent the three fundamental types of geometric curvature—zero, negative, and positive. Each space captures different structural relationships within the data, enabling the model to better adapt to the diverse patterns present in synthetic speech, such as linear trends, hierarchical manipulations, and cyclical emotional shifts. By jointly leveraging these complementary manifolds, **MiCuNet**

gains greater flexibility and robustness in representing fine-grained emotional and manipulation cues across languages. The total number of trainable parameters varies between 3.8M and 5.6M, contingent on the dimensionality of the input representations.

4 Experiments

4.1 Dataset

For our experiments, we utilize the EmoFake dataset by Zhao et al. (2024)⁸. The dataset includes recordings in two languages, English and Chinese. It features five emotional states: Neutral, Happy, Angry, Sad, and Surprise. A total of 20 speakers (10 English, 10 Chinese). Synthetic (fake) emotional speech samples are created using seven publicly available EVC models: VAW-GAN-CWT, DeepEST, Seq2Seq-EVC, CycleGAN-EVC, CycleTransGAN, EmoCycleGAN, and StarGAN-EVC. Each subset contains 27,300 training samples, 9,100 development samples, and 17,500 test samples. We adopt EmoFake as it uniquely provides aligned original/manipulated speech with generator labels across two languages. The EVC systems are part of the dataset specification (not selected by us); we follow the released protocols and splits.

Training Details: Our models undergo 50 epochs using the Adam optimization algorithm with a starting learning rate of 0.001 and mini-batches of 32 samples. For each of the three output tasks, we optimize the cross-entropy objective. To mitigate overfitting, we introduce dropout, gradually reduce the learning rate over time, and stop training early if validation performance degrades. We train and evaluate the models separately on the English and Chinese subsets. All experiments are conducted on a workstation equipped with an NVIDIA RTX 3080 Ti 12 GB GPU, an Intel® Core™ i9-10900K CPU, and 64 GB of RAM.

4.2 Experimental Results

In this section, we present the results of our experiments, reporting performance across multiple tasks and settings.

Baseline Performance: Table 1 presents the performance of individual pre-trained models (PTMs) and handcrafted spectral features evaluated separately on Original Emotion (OE), Current Emotion (CE), and Manipulation Source (M) across both

Fusion	Concatenation											
	(E-Tr) (E-Te)			(E-Tr) (C-Te)			(C-Tr) (C-Te)			(C-Tr) (E-Te)		
	OE	CE	M									
W2 + S-LI	3.60	2.15	3.05	5.16	3.21	4.32	3.83	2.26	3.24	4.62	2.81	3.98
W2 + S-ME	3.51	2.16	3.26	5.25	3.26	4.49	3.69	2.30	3.48	4.54	2.82	4.33
W2 + S-GT	3.52	2.36	3.39	5.41	3.38	4.57	3.74	2.52	3.58	4.55	3.04	4.39
W2 + C-ME	6.30	3.68	3.02	9.16	5.22	4.35	6.69	3.89	3.20	8.33	4.67	3.88
W2 + C-GT	4.87	2.82	3.63	7.05	4.14	5.11	5.20	2.98	3.83	6.33	3.62	4.77
W2 + C-LI	4.73	3.79	4.69	6.37	5.52	6.28	5.04	4.01	4.96	6.26	4.98	6.15
W2 + W-ME	5.48	4.70	4.81	7.45	6.36	7.27	5.79	4.96	5.09	7.19	6.13	6.36
W2 + W-GT	3.49	2.89	3.21	4.81	4.39	4.62	3.72	3.04	3.41	4.62	3.66	4.12
W2 + W-LI	5.19	3.13	4.57	7.27	4.63	6.27	5.51	3.29	4.80	6.80	4.03	5.98
WL + S-LI	3.82	2.23	3.16	5.21	3.25	4.36	4.02	2.35	3.32	4.97	2.93	4.07
WL + S-ME	3.93	2.26	2.98	5.33	3.32	4.55	4.15	2.41	3.18	5.13	2.94	3.97
WL + S-GT	3.62	2.50	3.43	5.51	3.44	4.63	3.83	2.66	3.64	4.70	3.26	4.39
WL + C-ME	6.87	3.60	2.97	9.31	5.31	4.44	7.35	3.82	3.16	8.99	4.67	3.90
WL + C-GT	5.08	2.78	3.66	7.13	4.19	5.20	5.36	2.94	3.91	6.56	3.63	4.73
WL + C-LI	4.41	3.68	4.43	6.44	5.61	6.34	4.71	3.92	4.68	5.86	4.76	5.76
WL + W-ME	5.13	4.51	5.43	7.58	6.43	7.40	5.44	4.76	5.76	6.60	5.84	7.05
WL + W-GT	3.19	3.08	3.18	4.87	4.45	4.66	3.40	3.28	3.40	4.16	4.02	4.11
WL + W-LI	5.52	3.47	4.49	7.39	4.71	6.38	5.87	3.70	4.78	7.10	4.55	5.96
MS + S-LI	1.62	1.02	1.45	2.32	1.48	1.99	1.73	1.09	1.54	2.12	1.31	1.92
MS + S-ME	1.64	1.01	1.43	2.23	1.50	2.10	1.73	1.06	1.52	2.15	1.32	1.88
MS + S-GT	1.77	1.11	1.38	2.54	1.62	2.03	1.87	1.17	1.45	2.29	1.43	1.78
MS + C-ME	3.13	1.55	1.44	4.42	2.33	2.02	3.34	1.64	1.52	4.15	1.98	1.89
MS + C-GT	2.41	1.37	1.58	3.34	1.92	2.35	2.58	1.46	1.66	3.11	1.78	2.02
MS + C-LI	2.09	1.73	1.95	3.00	2.43	2.85	2.23	1.84	2.08	2.72	2.21	2.58
MS + W-ME	2.43	2.06	2.23	3.36	2.85	3.29	2.56	2.20	2.38	3.16	2.66	2.97
MS + W-GT	1.52	1.45	1.54	2.23	2.01	2.18	1.61	1.54	1.63	1.99	1.91	1.96
MS + W-LI	2.13	1.47	1.96	3.27	2.13	2.80	2.24	1.56	2.07	2.72	1.88	2.50
XL + S-LI	2.34	1.48	1.99	3.26	2.07	2.79	2.48	1.56	2.11	2.99	1.92	2.62
XL + S-ME	2.37	1.43	2.01	3.17	2.02	2.82	2.52	1.50	2.12	3.07	1.83	2.62
XL + S-GT	2.33	1.57	1.90	3.43	2.19	2.83	2.48	1.66	2.02	3.10	2.01	2.49
XL + C-ME	4.05	2.20	1.97	5.91	3.29	2.71	4.27	2.32	2.10	5.14	2.81	2.62
XL + C-GT	3.11	1.82	2.32	4.48	2.56	3.22	3.31	1.94	2.44	4.09	2.35	2.93
XL + C-LI	2.90	2.45	2.94	4.01	3.43	3.94	3.05	2.57	3.12	3.75	3.20	3.88
XL + W-ME	3.13	2.85	3.26	4.53	3.83	4.41	3.34	2.99	3.43	4.02	3.72	4.15
XL + W-GT	2.13	1.97	2.06	3.06	2.77	2.93	2.28	2.10	2.17	2.82	2.52	2.69
XL + W-LI	3.32	2.11	2.57	4.51	2.87	3.95	3.55	2.22	2.73	4.38	2.73	3.34
W + S-LI	3.59	2.18	3.19	5.30	3.31	4.44	3.82	2.30	3.36	4.70	2.85	4.06
W + S-ME	3.71	2.42	3.32	5.41	3.35	4.63	3.93	2.55	3.55	4.90	3.18	4.33
W + S-GT	4.03	2.52	3.23	5.60	3.51	4.70	4.29	2.69	3.45	5.21	3.24	4.21
W + C-ME	7.03	3.75	3.37	9.46	5.39	4.52	7.49	3.97	3.55	9.00	4.84	4.31
W + C-GT	5.41	2.81	3.53	7.26	4.27	5.29	5.73	2.97	3.72	6.95	3.60	4.57
W + C-LI	4.59	4.14	4.53	6.57	5.70	6.46	4.90	4.41	4.82	5.91	5.47	5.87
W + W-ME	5.60	4.30	4.95	7.70	6.55	7.53	5.92	4.60	5.21	7.30	5.74	6.41
W + W-GT	3.45	3.19	3.52	4.95	4.53	4.75	3.63	3.35	3.74	4.47	4.09	4.64
W + W-LI	4.90	3.17	4.38	7.52	4.78	6.51	5.24	3.37	4.69	6.47	4.18	5.67
XV + S-LI	3.99	2.33	3.04	5.38	3.32	4.49	4.27	2.45	3.21	5.22	3.01	3.92
XV + S-ME	3.80	2.39	3.26	5.40	3.36	4.63	3.99	2.51	3.46	4.87	3.04	4.22
XV + S-GT	3.89	2.37	3.37	5.63	3.51	4.75	4.14	2.53	3.57	5.04	3.06	4.44
XV + C-ME	6.93	3.64	3.34	9.51	5.43	4.50	7.34	3.87	3.53	9.17	4.71	4.28
XV + C-GT	4.76	2.97	3.87	7.26	4.31	5.29	5.04	3.15	4.12	6.25	3.81	5.05
XV + C-LI	4.70	4.17	4.44	6.62	5.68	6.43	5.01	4.45	4.72	6.05	5.54	5.71
XV + W-ME	5.59	4.42	5.38	7.75	6.54	7.58	5.98	4.68	5.66	7.28	5.77	7.04
XV + W-GT	3.64	3.11	3.40	4.93	4.51	4.78	3.89	3.29	3.59	4.82	4.08	4.38
XV + W-LI	5.28	3.28	4.79	7.59	4.80	6.52	5.64	3.44	5.07	6.83	4.25	6.11

Table 2: Performance results using simple fusion concatenation on cross-lingual multitask prediction of Original Emotion (OE), Current Emotion (CE), and Manipulation Source (M). Results are reported as Equal Error Rates (EER %) using 5-fold cross-validation across four train-test language combinations. Color coding in the table highlights the top three performing configurations: blue (best), green (second best), and yellow (third best) based on lowest EER. consistent with the scheme used in Table 3.

English and Chinese corpora. Among all configurations, the Massively Multilingual Speech (MMS) model consistently delivers the strongest performance. On English CE, MMS achieves 87.45% accuracy, 86.98% F1, and an exceptionally low EER of 3.41%, with similarly high scores on OE

⁸<https://zenodo.org/records/12806228>

(81.90%, 80.44%, 5.29%) and M (85.22%, 83.10%, 3.95%). On the Chinese set, MMS maintains its lead, achieving 84.01% accuracy and 3.58% EER for CE, highlighting its robustness across languages and tasks. In the handcrafted domain, STFT-Linear (S-LI) emerges as a strong feature, achieving 81.23% accuracy and 3.53% EER on English CE, and 80.03% and 3.71% on Chinese CE—competitive with several PTMs. Features such as Wavelet-Gammatone (W-GT) and STFT-Mel (S-ME) also perform reliably across tasks, particularly in emotion classification, with EERs typically under 6%. Other PTMs, including Wav2Vec 2.0, WavLM, Whisper, and X-Vector, show moderate results and provide useful contrast for understanding the impact of multilingual training, model scale, and feature richness. These patterns reinforce the importance of both cross-lingual capacity and feature diversity, motivating the need for more sophisticated fusion strategies.

Multitask Performance: Table 2 extends the evaluation to a multitask setting using a straightforward concatenation of PTM embeddings and handcrafted features. Across all combinations, MMS paired with STFT-Mel (MS + S-ME) stands out as the top-performing setup. On English→English, it achieves 1.64% EER (OE), 1.01% (CE), and 1.43% (M)—a significant improvement over single-modality baselines. In transfer settings such as English→Chinese, it maintains strong results, with EERs of 2.23%, 1.50%, and 2.10%, respectively. Other combinations like MS + S-LI and MS + S-GT also perform well, consistently delivering EERs under 2.5% across most conditions. For example, MS + S-LI reaches 1.62%, 1.02%, and 1.45% on English→English, and remains competitive in cross-lingual settings. While simpler models such as Whisper or X-Vector show modest gains from concatenation, their performance remains limited compared to MMS-based pairings. These results confirm that simple fusion strategies can enhance multitask learning, especially when modalities are well-matched. However, the saturation of performance across different feature pairings indicates a need for more expressive fusion mechanisms, which **MiCuNet** addresses next. Table 3 reports results from the proposed MiCuNet framework, which performs curvature-aware fusion of PTM embeddings and spectral features across three geometric manifolds. The combination of MS + S-ME achieves the best overall performance, reaching 0.66% EER (OE), 0.31% (CE),

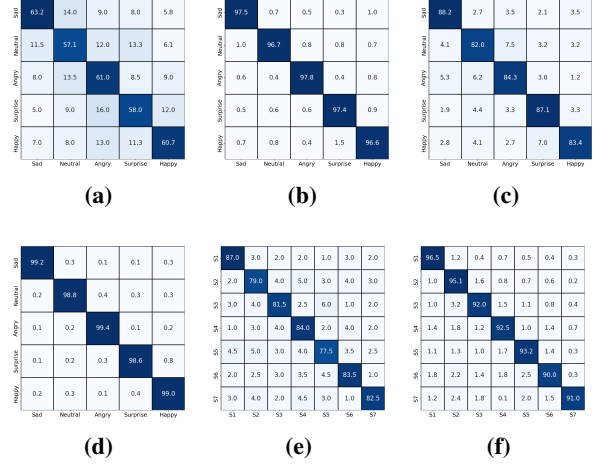


Figure 2: Confusion matrices across emotion and manipulation targets on the English subset. (a) OE classification using WavLM (singletask), (b) OE with **MiCuNet** using MMS + S-Mel (multitask), (c) CE with MMS + S-Mel (normal multitask), (d) CE with **MiCuNet** using MMS + S-Mel, (e) M classification using MMS + S-Mel (normal multitask), (f) M with **MiCuNet** using MMS + S-Mel. **MiCuNet** consistently improves class-wise separability, especially in multitask settings.

and 0.51% (M) on English→English. In cross-lingual scenarios, it continues to perform exceptionally well—for instance, 1.05%, 0.59%, 0.71% on English→Chinese, and 1.06%, 0.67, 0.95% on Chinese→English—demonstrating robust generalization. Other fusion combinations within MiCuNet, such as MS + S-LI and MS + S-GT, also deliver strong performance, with EERs frequently below 1.5% across multiple conditions. These results indicate that MiCuNet not only leverages the strengths of multilingual PTMs but also effectively aligns handcrafted spectral cues through its mixed-curvature projection and adaptive fusion strategy. Along with high performance the average inference time for MiCuNet is within range 1.2-1.6 seconds. Furthermore, the benefits of **MiCuNet** extend beyond the top-performing PTM. Even when applied to embeddings from models like WavLM or XLS-R, **MiCuNet** consistently reduces error rates, showing its flexibility across architectures and input types.

Visualization Analysis: We present confusion matrices and t-SNE visualizations to qualitatively assess model behaviour across OE, CE, and M targets on the English subset. Figure 2 shows confusion matrices for both single-task and multi-task settings. Subfigures 2a, 2c, and 2e display baseline results using WavLM and MMS, while 2b, 2d, and 2f correspond to the proposed **MiCuNet** with

Fusion	MiCuNet											
	(E-Tr) (E-Te)			(E-Tr) (C-Te)			(C-Tr) (C-Te)			(C-Tr) (E-Te)		
	OE	CE	M									
	1.90	1.17	1.65	2.88	1.75	2.31	1.96	1.26	1.63	1.58	2.41	2.18
W2 + S-LI	1.78	1.17	1.93	3.14	1.93	2.32	1.89	1.20	1.75	1.47	2.51	2.26
W2 + S-ME	1.89	1.39	1.99	2.96	1.71	2.55	1.95	1.45	1.98	1.65	2.72	2.36
W2 + C-ME	3.55	2.09	1.64	4.59	2.90	2.57	3.91	2.25	1.71	2.68	4.61	2.23
W2 + C-GT	2.87	1.65	1.94	4.09	2.43	2.88	3.07	1.54	1.98	2.14	3.18	2.64
W2 + C-LI	2.55	1.90	2.47	3.64	3.29	3.69	2.96	2.29	2.82	2.78	3.72	3.26
W2 + W-ME	3.28	2.54	2.49	3.97	3.81	4.17	2.92	2.61	2.93	3.32	3.89	3.45
W2 + W-GT	1.76	1.67	1.78	2.55	2.26	2.63	2.08	1.58	1.75	1.98	2.36	2.19
W2 + W-LI	2.85	1.65	2.31	4.05	2.48	3.38	3.14	1.97	2.56	2.30	3.66	3.33
WL + S-LI	2.02	1.16	1.86	2.75	1.65	2.18	2.06	1.37	1.94	1.58	2.92	2.10
WL + S-ME	2.13	1.17	1.67	2.83	1.97	2.52	2.13	1.27	1.60	1.51	3.07	2.24
WL + S-GT	2.11	1.32	1.88	3.20	2.05	2.77	2.21	1.38	2.06	1.65	2.49	2.62
WL + C-ME	3.47	2.09	1.56	5.37	2.93	2.55	4.09	2.27	1.80	2.48	5.05	2.27
WL + C-GT	3.01	1.66	1.95	3.90	2.32	2.65	3.10	1.47	2.09	2.08	3.92	2.48
WL + C-LI	2.48	2.09	2.40	3.46	2.90	3.25	2.45	2.24	2.72	2.40	3.11	3.33
WL + W-ME	3.02	2.32	2.98	4.00	3.77	4.15	3.16	2.59	3.37	3.22	3.73	3.57
WL + W-GT	1.68	1.61	1.62	2.62	2.63	2.50	2.12	1.53	1.96	2.16	2.76	2.09
WL + W-LI	2.88	1.85	2.57	4.39	3.55	3.52	3.01	1.86	2.71	2.29	4.10	3.01
MS + S-LI	0.77	0.46	0.62	1.10	0.67	0.86	0.82	0.72	0.75	0.79	1.12	1.10
MS + S-ME	0.66	0.31	0.51	1.05	0.59	0.71	0.78	0.40	0.70	0.67	1.06	0.95
MS + S-GT	1.05	0.66	0.74	1.42	0.93	1.10	0.99	0.60	0.83	0.84	1.36	1.01
MS + C-ME	1.76	0.89	0.78	2.49	1.33	1.17	1.99	0.91	0.79	1.17	2.27	1.08
MS + C-GT	1.21	0.74	0.85	1.86	1.15	1.29	1.37	0.80	0.95	1.05	1.74	1.02
MS + C-LI	1.07	1.01	1.06	1.54	1.35	1.58	1.25	0.97	1.06	1.17	1.44	1.46
MS + W-ME	1.24	1.07	1.16	1.80	1.66	1.84	1.43	1.31	1.37	1.37	1.89	1.50
MS + W-GT	0.86	0.82	0.92	1.25	1.17	1.11	0.81	0.91	0.84	1.06	1.13	1.13
MS + W-LI	1.27	0.79	1.17	1.94	1.19	1.61	1.29	0.90	1.21	1.13	1.60	1.35
XL + S-LI	1.25	0.85	1.09	1.78	1.15	1.59	1.39	0.83	1.19	0.99	1.52	1.56
XL + S-ME	1.34	0.82	1.04	1.59	1.01	1.44	1.26	0.86	1.22	1.08	1.55	1.51
XL + S-GT	1.38	0.83	1.00	1.96	1.12	1.59	1.30	0.93	1.16	1.17	1.72	1.42
XL + C-ME	2.31	1.30	1.15	3.47	1.84	1.46	2.18	1.30	1.06	1.53	2.94	1.42
XL + C-GT	1.74	0.93	1.26	2.48	1.47	1.80	1.82	1.12	1.39	1.32	2.24	1.54
XL + C-LI	1.47	1.39	1.51	2.30	2.04	2.19	1.72	1.52	1.64	1.70	2.02	2.05
XL + W-ME	1.75	1.68	1.95	2.44	2.17	2.52	1.97	1.73	1.86	1.97	2.14	2.10
XL + W-GT	1.14	1.18	1.11	1.54	1.50	1.75	1.18	1.11	1.19	1.43	1.47	1.59
XL + W-LI	1.82	1.17	1.36	2.60	1.70	2.21	1.82	1.19	1.47	1.60	2.20	1.71
W + S-LI	1.84	1.27	1.77	3.10	1.69	2.37	2.26	1.28	1.78	1.64	2.80	2.41
W + S-ME	1.89	1.44	1.75	2.88	1.71	2.53	1.97	1.45	2.00	1.76	2.75	2.17
W + S-GT	2.29	1.47	1.72	3.02	2.08	2.60	2.47	1.54	1.89	1.82	2.89	2.38
W + C-ME	3.59	1.88	1.76	5.36	2.86	2.65	4.31	2.36	1.98	2.65	4.70	2.17
W + C-GT	3.19	1.65	1.91	3.74	2.24	2.68	3.21	1.49	2.09	2.11	3.69	2.44
W + C-LI	2.71	2.13	2.49	3.78	3.09	3.77	2.91	2.27	2.67	3.22	3.28	2.95
W + W-ME	3.32	2.32	2.56	4.06	3.50	4.11	3.31	2.71	2.91	3.26	4.36	3.37
W + W-GT	1.88	1.88	1.86	2.50	2.43	2.80	2.17	1.72	2.04	2.29	2.45	2.61
W + W-LI	2.93	1.84	2.40	4.23	2.47	3.76	3.10	1.99	2.71	2.47	3.71	3.36
XV + S-LI	2.02	1.22	1.82	3.02	1.69	2.30	2.14	1.30	1.68	1.70	2.87	2.20
XV + S-ME	2.18	1.35	1.79	3.09	1.79	2.54	2.33	1.48	2.06	1.53	2.92	2.46
XV + S-GT	2.30	1.28	1.72	2.83	1.85	2.61	2.26	1.44	1.81	1.68	2.89	2.27
XV + C-ME	3.61	1.83	1.78	5.50	3.13	2.63	4.19	1.96	1.96	2.59	4.79	2.21
XV + C-GT	2.65	1.74	2.00	4.28	2.23	3.09	2.99	1.79	2.30	2.24	3.39	2.91
XV + C-LI	2.76	2.25	2.23	3.71	2.88	3.70	2.76	2.56	2.81	2.97	3.38	3.21
XV + W-ME	3.13	2.57	2.83	4.27	3.58	4.55	3.55	2.61	3.28	2.92	4.21	3.62
XV + W-GT	2.13	1.62	1.83	2.60	2.65	2.56	2.15	1.71	1.83	2.43	2.75	2.31
XV + W-LI	3.08	1.83	2.82	4.19	2.49	3.34	3.15	1.81	2.85	2.33	3.49	3.22

Table 3: Performance result using proposed fusion approach **MiCuNet** on Cross-lingual multitask performance for CE, OE, and source (M) prediction. Results are reported as 5-fold cross in metrics Equal Error Rates (EER %) across different train-test language combinations.

MMS + S-Mel. To better understand how different representations behave across the OE, CE, and M tasks, we present t-SNE visualizations of the fused embedding space on the English subset in Figure 3. Subfigures 3a, 3c, and 3e correspond to x-vector embeddings, while 3b, 3d, and 3f show results from the proposed **MiCuNet** using MMS + S-Mel fusion. Compared to x-vector, the **MiCuNet** representations exhibit clearer cluster boundaries

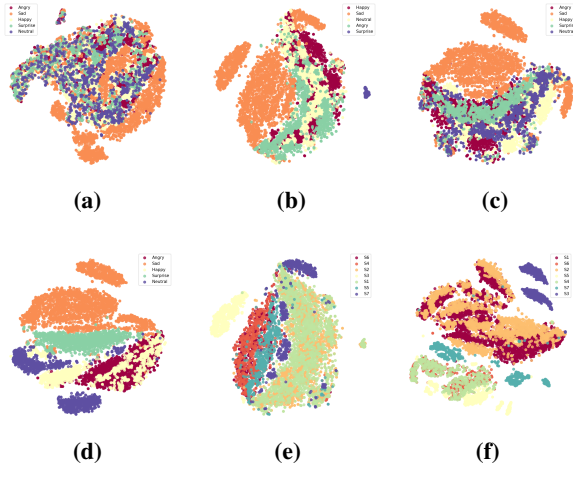


Figure 3: t-SNE visualizations of learned embeddings. x-vector — (a) OE, (c) CE, (e) Model. **MiCuNet** using MMS + S-Mel — (b) OE, (d) CE, (f) Model.

and more compact class-wise distributions across all targets, suggesting that the geometry-aware fusion effectively enhances task-relevant separability in the learned feature space. Model refers to the manipulation source—the specific EVC generators.

Evaluation Metrics: We evaluate each task using Accuracy, macro-F1, and Equal Error Rate (EER). Since EER is initially defined for binary classifications, we extend it to multi-class settings using a macro one-vs-rest formulation.

4.3 Ablation Study

To assess the contribution of individual geometric components and the learnable gating mechanism in **MiCuNet**, we conduct targeted ablation experiments. The results are summarized in Table 4,5,6.

Impact of Geometric Manifolds: We evaluate the importance of each geometric space by removing the Hyperbolic (-H) or Spherical (-S) branch from the fusion module. Excluding either leads to performance drops across tasks and languages, with the Hyperbolic space having a stronger impact. When both are removed (-H -S), leaving only the Euclidean branch, performance degrades further—highlighting the value of curved manifolds in capturing emotional and manipulation patterns.

Effect of Gating Mechanism: We further evaluate the role of the learnable gating module by replacing it with uniform averaging over the three manifolds (No Gating). Table 4 summarizes the impact of each architectural component on performance. **Generalization to Unseen EVC Sources:** To evaluate the robustness of **MiCuNet** to previously un-

Configuration	E → E			C → C		
	OE	CE	M	OE	CE	M
MiCuNet	0.66	0.31	0.51	0.78	0.40	0.70
Without Spherical (-S)	0.81	0.39	0.59	1.17	0.67	0.79
Without Hyperbolic (-H)	0.88	0.46	0.63	1.28	0.72	0.86
Only Euclidean (-H-S)	1.68	1.08	0.51	1.78	1.02	1.55
No Learnable Gating	2.76	2.41	2.59	3.20	3.63	3.80

Table 4: Ablation study on MiCuNet using MMS + S-MEL showing Equal Error Rate (%) for Original Emotion (OE), Current Emotion (CE), and Manipulation Source (M).

seen manipulation methods, we conduct a leave-two-out evaluation across the seven emotional voice conversion (EVC) models. In each case, the model is trained on speech generated by five EVC converters and tested exclusively on samples from the remaining two (S6 and S7), which are held out during training. Table 5 reports performance for both Original Emotion (OE) and Current Emotion (CE) predictions within the same language—English (E→E) and Chinese (C→C). Despite never encountering S6 or S7 during training. Table 6 extends this evaluation to cross-lingual settings, where models trained on one language are evaluated on another (E→C and C→E).

Model	E → E				C → C			
	S6		S7		S6		S7	
	OE	CE	OE	CE	OE	CE	OE	CE
MMS + S-MEL	1.78	1.20	1.69	1.21	1.84	1.39	1.77	1.26

Table 5: EER (%) of MiCuNet on unseen EVC models (S6, S7) for OE and CE within the same language.

Model	E → C				C → E			
	S6		S7		S6		S7	
	OE	CE	OE	CE	OE	CE	OE	CE
MMS + S-ME	1.95	1.88	1.91	1.56	2.31	2.00	2.17	1.98

Table 6: Cross-lingual EER (%) of MiCuNet on unseen EVC models (S6, S7) for OE and CE, with training and testing across different languages.

5 Conclusion

In this work, we addressed the task of tracing of emotional and manipulation attributes in synthetically generated speech. We introduced **MiCuNet**, a multitask framework that fuses speech foundation model (SFM) embeddings with spectrogram-based auditory features using a mixed-curvature projection strategy. By mapping representations across hyperbolic, Euclidean, and spherical spaces with a learnable gating mechanism, MiCuNet effectively captures complementary cues critical for emotion

and manipulation source inference. Evaluations on the EmoFake dataset across English and Chinese demonstrate that **MiCuNet** consistently outperforms conventional fusion baselines on all tasks, including original emotion, current emotion, and manipulation source prediction. Our findings underscore the value of using curvature-aware representations for understanding synthetic speech.

Ethical Statement

This work is conducted with the intent to improve transparency, accountability, and forensic analysis in the context of synthetic speech technologies. While the techniques developed in this study can detect and trace emotional manipulation in speech, we acknowledge that such technologies may also raise ethical concerns around surveillance, privacy, and potential misuse. All experiments were performed on publicly available datasets, and no human subjects were directly involved.

Limitation

The most significant limitation of this study lies in the lack of publicly available datasets explicitly designed for emotional manipulation in synthetic speech. To the best of our knowledge, EmoFake is the only publicly available dataset that includes parallel annotations for original emotion, manipulated emotion, and the conversion source. This scarcity of data limits the ability to perform broader benchmarking and evaluate cross-dataset generalization in more diverse and realistic settings. This makes comprehensive benchmarking and cross-dataset generalization challenging at this stage.

References

Jont B Allen and Lawrence R Rabiner. 1977. A unified approach to short-time fourier analysis and synthesis. *Proceedings of the IEEE*, 65(11):1558–1564.

Keith April Araño, Carlotta Orsenigo, Mauricio Soto, and Carlo Vercellis. 2021. Multimodal sentiment and emotion recognition in hyperbolic space. *Expert Systems with Applications*, 184:115507.

Arun Babu, Changhan Wang, Andros Tjandra, Kushal Lakhotia, Qiantong Xu, Naman Goyal, Kritika Singh, Patrick von Platen, Yatharth Saraf, Juan Pino, Alexei Baevski, Alexis Conneau, and Michael Auli. 2022. Xls-r: Self-supervised cross-lingual speech representation learning at scale. In *Interspeech 2022*, pages 2278–2282.

Alexei Baevski, Yuhao Zhou, Abdelrahman Mohamed, and Michael Auli. 2020. wav2vec 2.0: A framework for self-supervised learning of speech representations. *Advances in neural information processing systems*, 33:12449–12460.

Imen Baklouti, Olfa Ben Ahmed, and Christine Fernandez-Maloigne. 2024. **Cross-lingual low-resources speech emotion recognition with domain adaptive transfer learning**. In *Proceedings of the 13th International Conference on Data Science, Technology and Applications - Volume 1: DATA*, pages 118–128. INSTICC, SciTePress.

Judith C Brown. 1991. Calculation of a constant q spectral transform. *The Journal of the Acoustical Society of America*, 89(1):425–434.

Haozhe Chen, Run Chen, and Julia Hirschberg. 2024. **Emoknob: Enhance voice cloning with fine-grained emotion control**. In *Proceedings of the 2024 Conference on Empirical Methods in Natural Language Processing*, pages 8170–8180, Miami, Florida, USA. Association for Computational Linguistics.

Maximillian Chen and Zhou Yu. 2023. **Pre-finetuning for few-shot emotional speech recognition**. In *Interspeech 2023*, pages 3602–3606.

Sanyuan Chen, Chengyi Wang, Zhengyang Chen, Yu Wu, Shujie Liu, Zhuo Chen, Jinyu Li, Naoyuki Kanda, Takuya Yoshioka, Xiong Xiao, and 1 others. 2022. Wavlm: Large-scale self-supervised pre-training for full stack speech processing. *IEEE Journal of Selected Topics in Signal Processing*, 16(6):1505–1518.

Zengzhao Chen, Chuan Liu, Zhifeng Wang, Chuanxu Zhao, Mengting Lin, and Qiuyu Zheng. 2025. **Mtlser: Multi-task learning enhanced speech emotion recognition with pre-trained acoustic model**. *Expert Systems with Applications*, 273:126855.

Zhichen Han, Tianqi Geng, Hui Feng, Jiahong Yuan, Korin Richmond, and Yuanchao Li. 2025. **Cross-lingual speech emotion recognition: Humans vs. self-supervised models**. In *ICASSP 2025 - 2025 IEEE International Conference on Acoustics, Speech and Signal Processing (ICASSP)*, pages 1–5.

Tomi Kinnunen, Md. Sahidullah, Héctor Delgado, and 1 others. 2017. **The ASVspoof 2017 Challenge: Assessing the Limits of Replay Spoofing Attack Detection**. In *Proc. Interspeech 2017*, pages 2–6.

Yuke Li, Xinfu Zhu, Yi Lei, Hai Li, Junhui Liu, Danning Xie, and Lei Xie. 2023. **Zero-shot emotion transfer for cross-lingual speech synthesis**. In *2023 IEEE Automatic Speech Recognition and Understanding Workshop (ASRU)*, pages 1–8.

Stephane G Mallat. 1989. A theory for multiresolution signal decomposition: the wavelet representation. *IEEE transactions on pattern analysis and machine intelligence*, 11(7):674–693.

Nicolas M. Müller, Piotr Kawa, Wei Herng Choong, Edresson Casanova, Eren Gölge, Thorsten Müller, Piotr Syga, Philip Sperl, and Konstantin Böttiger. 2024. **Mlaad: The multi-language audio anti-spoofing dataset**. In *2024 International Joint Conference on Neural Networks (IJCNN)*, pages 1–7.

Vineel Pratap, Andros Tjandra, Bowen Shi, Paden Tomasello, Arun Babu, Sayani Kundu, Ali Elkahky, Zhaoheng Ni, Apoorv Vyas, Maryam Fazel-Zarandi, and 1 others. 2024. Scaling speech technology to 1,000+ languages. *Journal of Machine Learning Research*, 25(97):1–52.

Tianhua Qi, Shiyan Wang, Cheng Lu, Yan Zhao, Yuan Zong, and Wenming Zheng. 2024. **Towards realistic emotional voice conversion using controllable emotional intensity**. In *Interspeech 2024*, pages 202–206.

Alec Radford, Jong Wook Kim, Tao Xu, Greg Brockman, Christine McLeavey, and Ilya Sutskever. 2023. Robust speech recognition via large-scale weak supervision. In *International conference on machine learning*, pages 28492–28518. PMLR.

David Snyder, Daniel Garcia-Romero, Gregory Sell, Daniel Povey, and Sanjeev Khudanpur. 2018. X-vectors: Robust dnn embeddings for speaker recognition. *2018 IEEE International Conference on Acoustics, Speech and Signal Processing (ICASSP)*, pages 5329–5333.

Linhui Sun, Yunlong Lei, Zixiao Zhang, Yi Tang, Jing Wang, Lei Ye, and Pingan Li. 2025. **Multi-task coordinate attention gating network for speech emotion recognition under noisy circumstances**. *Biomedical Signal Processing and Control*, 107:107811.

Massimiliano Todisco, Xin Wang, Ville Vestman, and 1 others. 2019. **ASVspoof 2019: Future Horizons in Spoofed and Fake Audio Detection**. In *Proc. Interspeech 2019*, pages 1008–1012.

Shreya G. Upadhyay, Carlos Busso, and Chi-Chun Lee. 2024. **A layer-anchoring strategy for enhancing cross-lingual speech emotion recognition**. In *Interspeech 2024*, pages 4693–4697.

Chun Wang and Xizhong Shen. 2024. **Feature-enhanced multi-task learning for speech emotion recognition using decision trees and lstm**. *Electronics*, 13(14).

Zhizheng Wu, Tomi Kinnunen, Nicholas Evans, and 1 others. 2015. **ASVspoof 2015: the first automatic speaker verification spoofing and countermeasures challenge**. In *Proc. Interspeech 2015*, pages 2037–2041.

Junichi Yamagishi, Xin Wang, Massimiliano Todisco, and 1 others. 2021. **ASVspoof 2021: accelerating progress in spoofed and deepfake speech detection**. In *Proc. 2021 Edition of the Automatic Speaker Verification and Spoofing Countermeasures Challenge*, pages 47–54.

Yan Zhao, Jiangyan Yi, Jianhua Tao, Chenglong Wang, and Yongfeng Dong. 2024. Emofake: An initial dataset for emotion fake audio detection. In *China National Conference on Chinese Computational Linguistics*, pages 419–433. Springer.

Xingfa Zhou, Min Li, Lan Yang, Rui Sun, Xin Wang, and Huayi Zhan. 2023. [Emotion prompting for speech emotion recognition](#). In *Interspeech 2023*, pages 3108–3112.

Xinfa Zhu, Yi Lei, Tao Li, Yongmao Zhang, Hongbin Zhou, Heng Lu, and Lei Xie. 2024. [Metts: Multilingual emotional text-to-speech by cross-speaker and cross-lingual emotion transfer](#). *IEEE/ACM Trans. Audio, Speech and Lang. Proc.*, 32:1506–1518.